STRAIN SOFTENING WITH CREEP AND EXPONENTIAL ALGORITHM

By Zdeněk P. Bažant,[1] F. ASCE and Jenn-Chuan Chern[2]

ABSTRACT: A constitutive relation that can describe tensile strain softening with or without simultaneous creep and shrinkage is presented, and an efficient time-step numerical integration algorithm, called the exponential algorithm, is developed. Microcracking that causes strain softening is permitted to take place only within three orthogonal planes. This allows the description of strain softening by independent algebraic relations for each of three orthogonal directions, including independent unloading and reloading behavior. The strain due to strain softening is considered as additive to the strain due to creep, shrinkage and elastic deformation. The time-step formulas for numerical integration of strain softening are obtained by an exact solution of a first-order linear differential equation for stress, whose coefficients are assumed to be constant during the time step but may vary discontinuously between the steps. This algorithm is unconditionally stable and accurate even for very large time steps, and guarantees that the stress is always reduced exactly to zero as the normal tensile strain becomes very large. This algorithm, called exponential because its formulas involve exponential functions, may be combined with the well-known exponential algorithm for linear aging rate-type creep. The strain-softening model can satisfactorily represent the test data available in the literature.

INTRODUCTION

It is now well-established that a realistic prediction of long-time deformations and stress redistributions in concrete structures must take into account not only creep and shrinkage, but also cracking (1,18, 24,25,29,34). The previous works have, however, made one or more of the following unrealistic oversimplifications: (1) Cracking was modeled by a sudden stress reduction to zero when the tensile strength was reached; (2) creep of the material between the cracks was neglected; or (3) the aging effect was disregarded. The purpose of this study is to present a mathematical model which avoids all these oversimplifications.

Instead of a sudden stress reduction to zero after the attainment of the strength limit, one should consider the gradual strain softening of concrete, i.e., a gradual decline of stress at increasing strain. In a previous study (17), it was shown that cracks produced by drying are normally so fine and densely distributed, or so strongly restrained by adjacent compressed concrete, that a sudden formation of continuous cracks is impossible. At the same time, studies of fracture test data of concrete showed that strain-softening stress-strain relations are inevitable for describing the observed deviations from linear elastic fracture mechanics

[1]Prof. of Civ. Engrg. and Dir., Center for Concrete and Geomaterials, The Technological Inst., Northwestern Univ., Evanston, Ill. 60201.

[2]Grad. Research Asst., Northwestern Univ.; presently Postdoctoral Research Assoc., Div. of Reactor Analysis and Safety, Argonne National Lab., Argonne, Ill. 60439.

Note.—Discussion open until August 1, 1985. To extend the closing date one month, a written request must be filed with the ASCE Manager of Journals. The manuscript for this paper was submitted for review and possible publication on June 1, 1984. This paper is part of the *Journal of Engineering Mechanics*, Vol. 111, No. 3, March, 1985. ©ASCE, ISSN 0733-9399/85/0003-0391/$01.00. Paper No. 19541.

or from strength criteria, and for obtaining the correct structural size effect (12,31). Also, it has been found that the same strain-softening stress-strain relations yield correct deflections of reinforced concrete beams in the cracking stage (10), and explain the existing test data on the shear transmission across cracks with the associated dilatancy (8). Thus, the tensile strain softening—a property well-established experimentally (19,21–23,25,26,31)—emerges as a fundamental property of concrete. Our objective is to take it into account in creep analysis.

From experience, the numerical creep analysis of aging structures with a broad relaxation spectrum runs into difficulties with numerical stability and accuracy unless special techniques are adopted. The numerical analysis of strain-softening structures is even more notorious in that respect. Therefore, the objective of this paper is not only to set up a constitutive relation, but also to develop a stable, convergent, efficient and accurate algorithm for numerical integration.

The questions of spurious mesh sensitivity and incorrect convergence at mesh refinement, as well as the fracture mechanics aspects of strain softening (6,12,13), have to be left aside. We must keep in mind, though, that the present strain-softening relation can only be an overall property of a finite representative volume of heterogeneous material, not a point property of homogenized continuum. For the method of implementation in finite element programs, see Refs. 6 and 12.

OBJECTIVES AND FORMULATION OF CONSTITUTIVE RELATION

We seek a constitutive relation satisfying the following requirements:

1. In the absence of cracking or strain softening, the constitutive relation must reduce to that for linearly visco-elastic aging creep, augmented by the shrinkage and thermal expansion terms.
2. In the absence of creep (e.g., for very fast deformations), the constitutive relation must reduce to an algebraic stress-strain relation which describes strain softening.
3. Regardless of creep, aging, shrinkage and the loading path and history, the maximum principal tensile stress must reduce at very large tensile strain exactly to zero.

Requirement 3 is crucial. It makes it difficult to use for the deformations due to microcracking various incremental laws, such as those patterned after the theory of plasticity with loading surfaces, because such laws are path-dependent, whereas the final value of stress must always be zero regardless of the loading path. This condition may be satisfied if the stress-strain relation governing the strain-softening part of response is algebraic.

Should the algebraic relation between stress σ and strain ξ associated with strain softening and the stress-strain relation for creep and shrinkage be coupled in parallel or in series? (These two coupling modes are the only simple ones.) It is easy to verify that, for parallel coupling, requirement 3 cannot be attained. This was covered in a previous work (12), in which it was shown that a series coupling must be used. For this coupling, illustrated in Fig. 1(*a*), the stresses in the element repre-

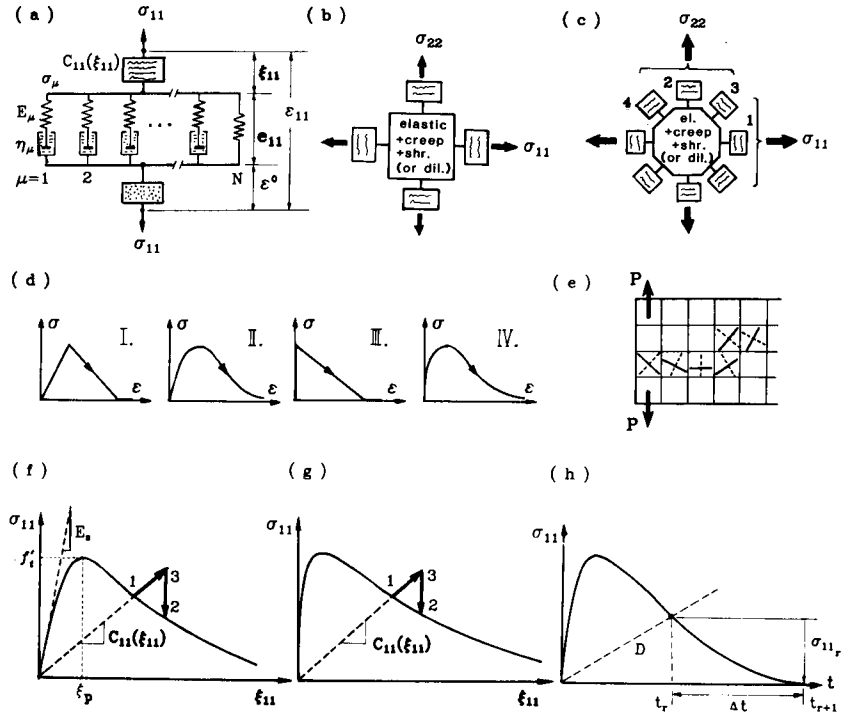

FIG. 1.—Rheologic Models, Strain-Softening Curves and Explanation of Time-Step Formulas

senting strain softening and those in the element representing creep with elasticity and shrinkage (or thermal dilatation) must be the same, and their respective deformations, ξ, e and ϵ^0, must be added. So we may write [see Fig. 1(*a*)]

$$\boldsymbol{\epsilon} = \mathbf{e} + \boldsymbol{\xi} + \boldsymbol{\epsilon}^0 \quad \ldots\ldots (1)$$

in which $\boldsymbol{\epsilon}$, $\mathbf{e}$, $\boldsymbol{\xi}$ and $\boldsymbol{\epsilon}^0$ = column matrices of the cartesian components of the tensors of total strain, of strain due to elastic deformation and creep, of strain associated with strain softening, and of the strain due to shrinkage or thermal dilatation, respectively. In terms of the components, $\boldsymbol{\epsilon} = (\epsilon_{11}, \epsilon_{22}, \epsilon_{33}, \epsilon_{12}, \epsilon_{23}, \epsilon_{31})^T$; $\boldsymbol{\sigma} = (\sigma_{11}, \sigma_{22}, \sigma_{33}, \sigma_{12}, \sigma_{23}, \sigma_{31})^T$; and $\boldsymbol{\xi} = (\xi_{11}, \xi_{22}, \xi_{33}, \xi_{12}, \xi_{23}, \xi_{31})^T$, ... in which the numerical subscripts refer to cartesian coordinates x_1, x_2 and x_3, and superscript T refers to a transpose of the matrix.

As argued, the relation between $\boldsymbol{\sigma}$ and $\boldsymbol{\xi}$ must be algebraic (for monotonic loading), and so

$$\boldsymbol{\sigma} = \mathbf{C}(\boldsymbol{\xi})\boldsymbol{\xi} \quad \ldots\ldots (2)$$

C represents a 6 × 6 matrix formed by the cartesian components of th secant moduli tensor; C is a function of $\boldsymbol{\xi}$. The form of this function fc arbitrary multiaxial deformation paths is difficult to determine. In this

regard, we adopt here the following simplifying hypothesis.

Hypothesis I.—At each point of the material, cracks or microcracks are permitted to form only in three mutually orthogonal planes, i.e., no other crack directions are permitted. These planes can have any orientation; however, this orientation must be kept fixed after deformations due to strain softening (cracking) begin.

This hypothesis, illustrated in Fig. 1(*b*), suffices for many practical situations and simplifies the mathematics because orthogonal cracks do not interact. It would, of course, be more realistic to also permit various inclined crack orientations, as shown in Fig. 1(*c*). Then, however, all cracks forming a skew angle with a certain direction contribute to the overall deformation in that direction, i.e., cracks of various orientations interact. A mathematical model which takes such interactions into account has been conceived (11), and is planned for investigation later.

According to Hypothesis I, cracking normal to axis x_1 increases the overall deformation in the x_1 direction and has no effect on the deformations in other orthogonal directions [Fig. 1(*b*)]. Consequently, matrix C should have only the diagonal terms associated with normal strain, and all other elements of the matrix should be zero, i.e.:

$$\mathbf{C} = \begin{bmatrix} C_{11} & 0 & 0 & 0 & 0 & 0 \\ & C_{22} & 0 & 0 & 0 & 0 \\ & & C_{33} & 0 & 0 & 0 \\ \text{sym.} & & & 0 & 0 & 0 \\ & & & & 0 & 0 \\ & & & & & 0 \end{bmatrix} \quad \ldots\ldots (3)$$

in which $C_{11} = C(\xi_{11})$; $C_{22} = C(\xi_{22})$; and $C_{33} = C(\xi_{33})$. This means that, e.g.:

$$\sigma_{11} = C(\xi_{11})\xi_{11} \quad (11 \rightarrow 22 \rightarrow 33) \quad \ldots\ldots (4)$$

in which subscripts 11 can be permutated with 22 and 33 as indicated. According to requirement 3, function $C(\xi_{11})$ must be such that $\lim C = 0$ as $\xi_{11} \rightarrow \infty$. This function may be chosen to describe any one of the diagrams shown in Fig. 1(*d*) (bilinear or smooth, with either inclined or vertical initial slope).

In the step-by-step analysis of structures, the crack orientation can differ from one finite element to the next [Fig. 1(*e*)]. The crack orientation is fixed in each finite element at the time the maximum principal stress σ_I first attains a certain given critical value, σ_I^*, at which nonlinear deformation (cracking) begins. If the σ_{11}-ξ_{11} diagram is linear up to the peak, then $\sigma_I^* = f_t'$ = tensile strength. If it is curved before the peak, then $\sigma_I^* < f_t'$. If it is curved from the origin but the curvature is small up to, say, $0.7 f_t'$ (Eq. 26*a*), one may use, as an approximation, $\sigma_I^* \simeq 0.7 f_t'$.

Next we need to describe the linearly visco-elastic aging creep component, $\mathbf{e}$. It is usually characterized in terms of the compliance function $J(t,t')$ which can be directly measured or predicted from other properties (2,4). The constitutive law is then expressed on the basis of the superposition principle by means of a history integral. This form, however,

is inconvenient for numerical computations. Fortunately, it is known how to convert the most general integral-type creep law, based on the compliance function, to a rate-type form defined as a set of first-order ordinary differential equations in time (2,19). Various rate-type formulations are possible, and the one preferred is that visualized by the Maxwell chain model [Fig. 1(*a*)]. For this model, we have (2,5,19):

$$\boldsymbol{\sigma} = \sum_{\mu=1}^{N} \boldsymbol{\sigma}_\mu, \quad \dot{\mathbf{e}} = \frac{1}{E_\mu(t)} \mathbf{B}\dot{\boldsymbol{\sigma}}_\mu + \frac{1}{\eta_\mu(t)} \mathbf{B}'\boldsymbol{\sigma}_\mu \quad \ldots\ldots\ldots\ldots\ldots\ldots\ldots\ldots\ldots\ldots (5)$$

in which superior dots denote derivates with respect to time t; and E_μ and η_μ = the uniaxial spring moduli and dashpot viscosities associated with the individual units of the Maxwell chain, labeled by subscript $\mu = 1, \ldots N$. E_μ and η_μ depend on the age of concrete, t. An effective algorithm for determining E_μ and η_μ from given compliance functions is available (4). Column matrices $\boldsymbol{\sigma}_\mu$ represent the components of the stresses in the individual Maxwell chain units, called the partial stresses or hidden stresses: $\boldsymbol{\sigma}_\mu = (\sigma_{\mu_{11}}, \sigma_{\mu_{22}}, \ldots)^T$. Finally, $\mathbf{B}$ and $\mathbf{B}'$ = constant matrices defined as

$$\mathbf{B} = \mathbf{B}' = \begin{bmatrix} 1 & -\nu & -\nu & 0 & 0 & 0 \\ & +1 & -\nu & 0 & 0 & 0 \\ & & 1 & 0 & 0 & 0 \\ & & & 1+\nu & 0 & 0 \\ & & & & 1+\nu & 0 \\ \text{sym.} & & & & & 1+\nu \end{bmatrix} \quad \ldots\ldots\ldots\ldots\ldots (6)$$

in which ν represents the Poisson ratio of concrete (approximately 0.18). This ratio happens to be about the same for the elastic deformations and for the creep deformations, which is why $\mathbf{B}' = \mathbf{B}$. In general, $\mathbf{B}$ need not be equal to $\mathbf{B}'$, and then different values of ν would be used for $\mathbf{B}$ and $\mathbf{B}'$.

The structure of the matrix in Eq. 6 is a consequence of isotropy of the material. To satisfy isotropy conditions, the differential equations corresponding to the Maxwell chain are usually written separately for the volumetric and deviatoric components, using volumetric and deviatoric moduli and viscosities (18). By superimposing such equations, one obtains Eqs. 5 and 6, which are more convenient for our purpose.

The constitutive relation is now completely defined by Eqs. 1, 2 and 5. In this formulation, $\mathbf{e}$, $\boldsymbol{\xi}$ and $\boldsymbol{\sigma}_\mu$ are quantities which are not directly measurable, unlike strain $\boldsymbol{\epsilon}$ or stress $\boldsymbol{\sigma}$. Such quantities are called internal variables (or hidden variables).

It may be noted that our model, on the whole, uses neither series nor parallel coupling of individual components, but a mixture of the two, since the units of the Maxwell chain are coupled in parallel. Also note that if a generalization permitting inclined crack directions were introduced, then a further parallel coupling would have to be imposed on the cracking elements.

The structure of the constitutive equation reflects the different origins of inelastic strains. The Maxwell chain model describes the strain of intact concrete between the cracks, and the strain-softening elements [Fig. 1(*a*)] describe the additional accumulated macroscopic strain due to the progressive formation of cracks. If the cracks are assumed as continuous, parallel and planar, the deformation due to the cracks must be added to the deformation in intact concrete, and the stress transmitted by both should be the same, provided the cracks are restricted to three orthogonal directions.

After trying numerous variants of the temporal, numerical, step-by-step integration, it appeared suitable to treat the elastic-creep component and the strain-softening component separately, as we describe it now.

Exponential Algorithm for Strain Softening

Consider now solely the deformations due to strain softening. Differentiating Eq. 4, we get $\sigma_{11} = C_{11}\dot{\xi}_{11} + \dot{C}_{11}\xi_{11}$. We might be tempted to consider the last term as an inelastic stress rate, determined on the basis of the stress and strain state in the previous loading step or previous iteration of the current step. However, such an approach often appears unstable when the stress-strain relation has a negative slope, and, even if the computations remain stable, a large error is usually accumulated, with the result that the stress is not reduced exactly to zero at very large ξ_{11}.

An intuitive analogy with the Maxwell model for stress relaxation now appears to be helpful. The stress relaxation equations, as we know, always yield a zero stress value after the lapse of sufficient time. A relation which formally looks like the equation for the Maxwell model may be obtained by setting $\sigma_{11} = C_{11}\dot{\xi}_{11} + \dot{C}_{11}\xi_{11} = C_{11}\dot{\xi}_{11} + \dot{C}_{11}(\sigma_{11}/C_{11})$, which may be rewritten as

$$\dot{\sigma}_{11} + \frac{\sigma_{11}}{\beta_{11}} = C_{11_{r+1/2}}\dot{\xi}_{11} \quad \ldots\ldots\ldots\ldots\ldots\ldots\ldots\ldots\ldots\ldots\ldots\ldots\ldots\ldots (7)$$

where we introduce the notation $1/\beta_{11} = -\dot{C}_{11}/C_{11}$. In this equation it is most accurate to take the value of C_{11} for the middle of the time step (t_r, t_{r+1}) in which r is the number of the time step ($r = 1, \ldots 2 \ldots$). Thus, $C_{11_{r+1/2}} = 1/2(C_{11_r} + C_{11_{r+1}})$, in which the subscripts r, $r + 1$ and $r + 1/2$ refer to times t_r, t_{r+1} and the midstep time. Based on increment ΔC_{11}, the coefficient β_{11} may be approximated as

$$\frac{1}{\beta_{11}} = -\frac{\Delta C_{11}}{C_{11_{r+1/2}}\Delta t} \qquad (\Delta t = t_{r+1} - t_r) \ldots\ldots\ldots\ldots\ldots\ldots\ldots\ldots\ldots\ldots (8)$$

Since the tensile strength f_t' depends on age t, we have $C_{11} = C[\xi_{11}, f_t'(t)]$. Now there is a question of how to differentiate C, which is needed to evaluate β_{11}. To satisfy requirement 3, we cannot use $\Delta C_{11} = (\partial C/\partial \xi)\Delta\xi$; rather we must use the total difference $\Delta C_{11} = (\partial C/\partial \xi_{11})\partial\xi_{11} + (\partial C/\partial f_t')\Delta f_t'$. Similarly, if $C_{11} = C(\xi_{11}, T)$ in which T = temperature, we must use in Eq. 8 $\Delta C_{11} = (\partial C/\partial \xi_{11})\Delta\xi_{11} + (\partial C/\partial T)\Delta T$ in order to satisfy requirement 3 (except for unloading). This means that (for loading) the stress must always correspond to a path-independent secant modulus even if C depends on f_t' or T, or both.

Eq. 7 looks like an equation for stress relaxation, and we solve it as

such, assuming that during the time step Δt the values of the right-hand side of this equation and of β_{11} are constant, although they may vary by discontinuous jumps between the time steps. This approach is the same as that used in deriving the exponential algorithm for rate-type creep (2,5,19). The general solution of Eq. 7 is then exactly

$$\sigma_{11}(t) = Ae^{-(t-t_r)/\beta_{11}} + C_{11_{r+1/2}}\beta_{11}\dot{\xi}_{11} \quad \ldots\ldots (9)$$

in which A is an integration constant. From the initial condition $\sigma_{11} = \sigma_{11_r}$ at $t = t_r$, we get $A = \sigma_{11_r} - C_{11_{r+1/2}}\beta_{11}\dot{\xi}_{11}$, from which

$$\sigma_{11}(t) = \sigma_{11_r}e^{-(t-t_r)/\beta_{11}} + (1 - e^{-(t-t_r)/\beta_{11}})C_{11_{r+1/2}}\beta_{11}\dot{\xi}_{11} \quad \ldots\ldots (10)$$

For the end of the time step, $t = t_{r+1} = t_r + \Delta t$, we have

$$\sigma_{11_r} + \Delta\sigma_{11} = \sigma_{11_r}e^{-\Delta z_{11}} + \frac{1}{\Delta z_{11}}(1 - e^{-\Delta z_{11}})C_{11_{r+1/2}}\Delta\xi_{11} \quad \ldots\ldots (11)$$

in which we introduced the notation $\Delta z_{11} = \Delta t/\beta_{11} = -\Delta C_{11}/C_{11_{r+1/2}}$. Eq. 11 may be rewritten in the form of a pseudo-elastic stress-strain relation with initial strain $\Delta\xi''_{11}$, i.e., $\Delta\sigma_{11} = D_{11}(\Delta\xi_{11} - \Delta\xi''_{11})$ or

$$\Delta\xi_{11} = \frac{\Delta\sigma_{11}}{D_{11}} + \Delta\xi''_{11} \quad \ldots\ldots (12)$$

in which

$$D_{11} = \frac{1}{\Delta z_{11}}(1 - e^{-\Delta z_{11}})C_{11_{r+1/2}}, \quad \Delta\xi''_{11} = (1 - e^{-\Delta z_{11}})\frac{\sigma_{11_r}}{D_{11}} \quad \ldots\ldots (13)$$

D_{11} may be regarded as an incremental elastic modulus.

Eq. 12 may be written as $\Delta\sigma_{11} = \Delta\sigma^{el}_{11} - \Delta\sigma^{cr}_{11}$, in which $\Delta\sigma^{el}_{11} = D_{11}\Delta\xi_{11}$, $\Delta\sigma^{cr}_{11} = D_{11}\Delta\xi''_{11}$. The incremental relation may then be interpreted as shown in Fig. 1(f) and Fig. 1(g), in which the increment $\overline{13}$ is the elastic stress change at arrested cracking, $\Delta\sigma^{el}_{11}$, and the increment $\overline{32}$ is the inelastic stress relaxation at fixed deformation, $\Delta\sigma^{cr}_{11}$.

Let us now look at the limiting properties of Eq. 12. If the loading step is very small, $\Delta\xi_{11} \to 0$, the limiting values of Eq. 13 are

$$D_{11} \to C_{11_{r+1/2}}, \quad \Delta\xi''_{11} \to -\frac{\sigma_{11_r}\Delta C_{11}}{C^2_{11_{r+1/2}}} \quad \ldots\ldots (14)$$

Now compare this to the central difference approximation of Eq. 7, $\Delta\sigma_{11} + \Delta t(\sigma_{11_r} + \Delta\sigma_{11}/2)\beta_{11} = D_{11}\Delta\xi_{11}$, in which $D_{11} = C_{11}(t_{r+1/2})$. For very small Δt, we have $\Delta\sigma_{11} = C_{11}\Delta\xi_{11} - \sigma_{11}\Delta t/\beta_{11} = C_{11}(\Delta\xi_{11} - \Delta\xi''_{11})$ with $\Delta\xi''_{11} = \sigma_{11}\Delta t/(\beta_{11}C_{11})$, and because $\Delta t/\beta_{11} = -\Delta C_{11}/C_{11}$, we get $\Delta\xi''_{11} = -\sigma_{11}\Delta C_{11}/C^2_{11}$, which is the same as Eq. 14. Therefore, in the limit for very small loading steps, the exponential algorithm is equivalent to the central difference formulas. Thus, for very short diminishing time steps, our algorithm would converge in the same manner as that based on the central difference formula.

However, the foregoing formulas, which we will call the exponential formulas, are used because they permit very long time steps Δz_{11}. If $\Delta z_{11} \to \infty$, the right-hand side of Eq. 11 tends to 0, which guarantees that at very large strains the stress will be reduced to exactly zero, even

if some error is accumulated during previous loading steps. For comparison, consider again the aforementioned central difference approximation of Eq. 7, for which we have $\Delta\sigma_{11} = (D_{11}\Delta\xi_{11} - \sigma_{11_r}\Delta t/\beta_{11})/(1 + \Delta t/2\beta_{11})$, in which $D_{11} = C_{11}(t_{r+1/2})$. Now, for very large Δt, we get $\Delta\sigma_{11} = -2\sigma_{11_r}$, which means that the stress would overshoot an equal distance into the opposite stress values and would not be reduced to exactly zero at very large time steps. By contrast, for the exponential algorithm $\Delta\sigma_{11} = -\Delta\sigma^{cr}_{11} = -D_{11}\Delta\xi''_{11} = -\sigma_{11_r}$, i.e. the stress is reduced to exactly zero. Besides, $D_{11} \to 0$, which means that the stress, once reduced to zero, will remain zero for further loading [Fig. 1(h)].

Such characteristics of the solution are important for solving long-time creep effects in concrete structures with cracking. For steady loads, it is possible and, in fact, necessary to increase the time step in a geometric progression from very small initial values (needed because short relaxation times are present) to very long time steps (of the order of 1 yr) near the end of integration. If it happens that cracking begins after many years, suddenly the stresses begin changing rapidly during cracking. Yet it would be inconvenient to introduce very small time steps each time this happens. The present formulas with their long-term asymptotic properties make it possible to let this cracking happen within only a few time steps and still maintain reasonable accuracy.

Combining Eq. 12 with similar incremental relations for directions x_2 and x_3, we obtain the matrix incremental relation

$$\Delta\boldsymbol{\xi} = \mathbf{B}^C\Delta\boldsymbol{\sigma} + \Delta\boldsymbol{\xi}'' \quad \ldots\ldots (15)$$

in which $\mathbf{B}^C =$

$$\begin{bmatrix} D_{11}^{-1} & 0 & 0 & 0 & 0 & 0 \\ & D_{22}^{-1} & 0 & 0 & 0 & 0 \\ & & D_{33}^{-1} & 0 & 0 & 0 \\ & & & 0 & 0 & 0 \\ \text{sym.} & & & & 0 & 0 \\ & & & & & 0 \end{bmatrix} \quad \ldots\ldots (16)$$

Here the expressions for D_{22} and D_{33} are obtained from Eq. 13 by subscript permutations $11 \to 22 \to 33$, and the same permutations apply for the components of the column matrix $\Delta\boldsymbol{\xi}'' = (\Delta\xi''_{11}, \Delta\xi''_{22}, \Delta\xi''_{33}, 0, 0, 0)^T$.

An essential aspect for convergence and stability is the use of the secant modulus, C_{11}. If tangential formulas (in which $\Delta\xi''_{11} = 0$) were used, convergence and stability of iterations would not be obtained in the strain-softening region, as numerical experience indicated.

Exponential Algorithm for Rate-Type Creep

The preceding formulation of the exponential algorithm for strain softening is patterned after the exponential algorithm for rate-type aging creep developed in 1971 (2,3,5,7,19). For steady loads, this algorithm permits increasing the time step to values that are much larger than the shortest relaxation time, without any significant loss of accuracy. The time-step relations are derived as the exact integrals of the differential equations for the Maxwell chain under the assumption that the equa-

tion's coefficients are constant during the time step and change only by discontinuous jumps between the time steps. Taking the equations of this algorithm, as stated for the volumetric and deviatoric parts (e.g., on page 213 of Ref. 2, or in Ref. 19), and combining them in matrix form, we have

$$\Delta \mathbf{e} = \mathbf{B}^M \Delta \boldsymbol{\sigma} + \Delta \mathbf{e}'' \quad \ldots\ldots (17)$$

$$\Delta \mathbf{e}'' = \mathbf{B}^M \Delta \boldsymbol{\sigma}^M, \quad \mathbf{B}^M = \frac{1}{E^M}\mathbf{B} \quad \ldots\ldots (18)$$

$$E^M = \sum_{\mu} \lambda_\mu E_\mu(t_{r+1/2}), \quad \Delta \boldsymbol{\sigma}^M = \sum_{\mu} \boldsymbol{\sigma}_{\mu_r}(1 - e^{-\Delta y_\mu}) \quad \ldots\ldots (19)$$

$$\lambda_\mu = \frac{1}{\Delta y_\mu}(1 - e^{-\Delta y_\mu}), \quad \Delta y_\mu = \frac{\Delta t}{\tau_\mu^*}, \quad \tau_\mu^* = \left[\frac{\eta_\mu}{E_\mu}\right]_{r+1/2} \quad \ldots\ldots (20)$$

in which $\mu = 1, 2, \ldots N$; $\Delta \mathbf{e}''$ represents the column matrix of the inelastic strain increments due to creep, $\mathbf{B}^M$ is a square matrix of pseudo-elastic incremental compliances; and τ_μ^* are called the relaxation times. If temperature is constant, the values of τ_μ^* may be chosen as constants. They may be considered to be spaced in the logarithm of age by decades (2,3,5,7,19). The new values of the partial stresses are obtained from the relation

$$\boldsymbol{\sigma}_{\mu_{r+1}} = \boldsymbol{\sigma}_{\mu_{r+1}} e^{-\Delta y_\mu} + \lambda_\mu E_\mu(t_{r+1/2}) \mathbf{B}^{-1} \Delta \mathbf{e} \quad \ldots\ldots (21)$$

Note that, for very short time steps ($\Delta y_\mu \to 0$), this equation is equivalent to a central difference approximation of Eq. 5 for the Maxwell chain, while for a very long time step ($\Delta y_\mu \to \infty$), Eq. 21 always yields a zero stress value.

The incremental relations for elastic deformation with creep, strain softening and shrinkage (or thermal dilatation) may now be combined as $\Delta \boldsymbol{\epsilon} = \Delta e + \Delta \xi + \Delta \epsilon^0$. Substituting Eqs. 15 and 17, we obtain the following pseudo-elastic incremental stress-strain relation

$$\Delta \boldsymbol{\epsilon} = \mathbf{D} \Delta \boldsymbol{\sigma} + \Delta \boldsymbol{\epsilon}'' \quad \ldots\ldots (22)$$

$$\text{in which} \quad \mathbf{D} = \mathbf{B}^M + \mathbf{B}^C, \quad \Delta \boldsymbol{\epsilon}'' = \Delta \mathbf{e}'' + \Delta \boldsymbol{\xi}'' + \Delta \boldsymbol{\epsilon}^0 \quad \ldots\ldots (23)$$

$\mathbf{D}$ represents the overall incremental compliance matrix, from which the incremental stiffness matrix may be obtained by inversion; $\Delta \boldsymbol{\epsilon}''$ represents the column matrix of the total inelastic strain increments; and $\Delta \boldsymbol{\epsilon}^0$ is the given increment of shrinkage strain or thermal strain.

Strain-Softening Diagram, Unloading, Reloading

It is a typical property of fracturing materials that their elastic stiffness degrades due to fracturing. If the microcracks were perfectly smooth, without interlock and rubble inside the crack space, and if the matrix were perfectly elastic with no nonlinear regions at the crack tips, the material would have to unload according to the secant elastic moduli all the way to the origin of coordinates. Comparison with recent test data (28), however, reveals that this is not so. The initial unloading slope is

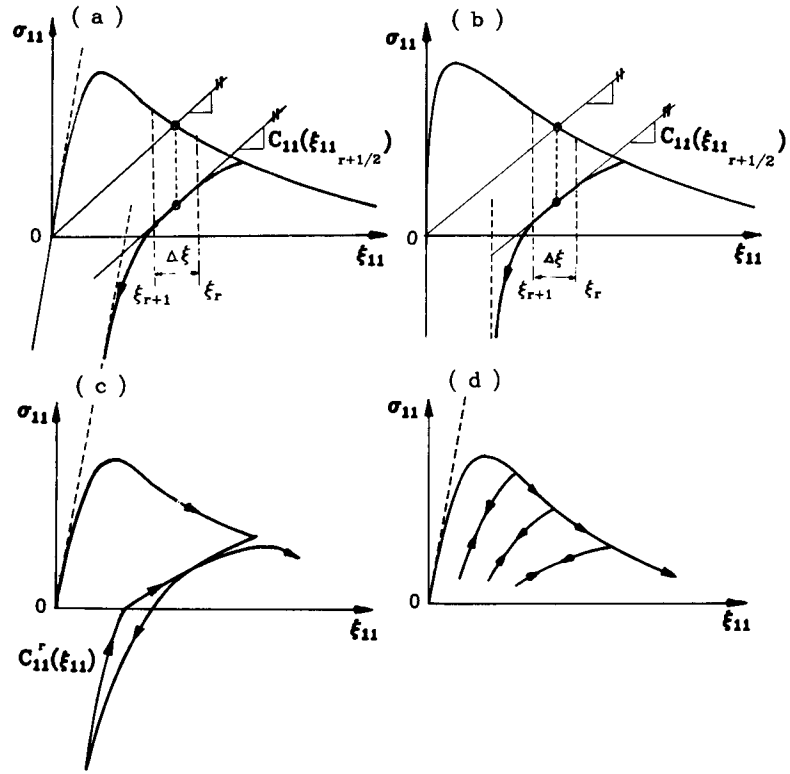

FIG. 2.—Unloading and Reloading Behavior Assumed

much steeper than the secant slope, although often still much smaller than the elastic modulus for virgin concrete [Fig. 2(*c*)]. During unloading, the material gradually stiffens and eventually regains its original elastic stiffness [Fig. 2(*c*)]. This happens at very large compressive stresses rather than at zero stress. The stiffening of the material is obviously due to the fact that cracks, once formed, cannot close completely, partly because of rubble and interlocking fragments within the crack space, and partly because of irreversible deformations in the nonlinear crack-tip regions.

Although more realistic (and more complicated) diagrams for unloading could be derived, it seems that the following simple rule works adequately for unloading:

$$\Delta \xi_{11}'' = 0 \quad \text{if} \quad \Delta \xi_{11} \le 0 \quad (11 \to 22 \to 33) \quad \ldots\ldots (24)$$

i.e., the increments of the fracturing strains ξ_{11}, given for loading by Eq. 13, are set equal to zero in the case of unloading. By virtue of the fact that we have only three possible crack directions, the unloading condition can be checked independently for each of the fracturing strains, ξ_{11}, ξ_{22} and ξ_{33}. The elastic moduli $C_{11}(\xi_{11})$, etc., as well as the moduli D_{11}, etc., in Eq. 13, for finite loading steps, are left unaffected

by unloading. They are evaluated from the current values of fracturing strains ξ_{11}, ... in the same manner as for loading, and due to finite steps the central difference formula is used, i.e., $C_{11} = C_{11_{r+1/2}} \simeq [C_{11}(\xi_r) + C_{11}(\xi_{r+1})]/2$.

The rule for generating the unloading diagram is shown geometrically in Figs. 2(*a*) and 2(*b*), for both the cases when the initial slope of the σ_{11}-ξ_{11} diagram is finite and infinite. The slope of the tangent of the unloading diagram at fracturing strain ξ_{11} is equal to the secant modulus of the loading diagram at the same value of ξ_{11}, i.e., the straight lines marked in Figs. 2(*a*) and 2(*b*) are parallel. It is easy to construct the unloading diagram geometrically according to this rule. The diagram obtained in this manner is, at the start of unloading, less steep than the test data indicate, but after some small unloading the slope roughly agrees with tests of unloading after tensile strain softening (28).

In a perfect elastic material without rubble and interlock in the cracks and without nonlinear crack-tip regions, the reloading would have to proceed along the same line as unloading, but this is not true in reality. At the beginning of reloading, the stiffness tends to be higher than the unloading stiffness at the same stress, but not higher than the initial slope of the virgin diagram. This is true as long as there is compression across the cracks. When reloading reaches the tensile region, then the reloading stiffness becomes smaller than the unloading stiffness at the same stress. This is true, however, only if the previous unloading reached compressive strains. The following simple empirical rule, which can again be implemented separately for each of the components ξ_{11}, ξ_{22} and ξ_{33}, appears to work acceptably:

$$C^r_{11}(\xi) = a_0 C_{11}(\xi_{11}) + (1 - a_0)C_{11}(0) \quad \text{for} \quad \sigma_{11} < 0$$

$$C^r_{11}(\xi) = a_1 C_{11}(\xi_{11}) + (1 - a_1)C_{11}(\xi_{11_{max}}) \quad \text{for} \quad \sigma_{11} > 0$$

$$(11 \rightarrow 22 \rightarrow 33) \qquad (25)$$

in which superscripts r refer to reloading, and a_0 and a_1 are reloading coefficients between 0 and 1 (typically $a_0 = a_1 = 0.5$). $\xi_{11_{max}}$ denotes the value of ξ_{11} when unloading began. After ξ_{11} reaches $\xi_{11_{max}}$, the virgin loading curve is again followed. When the unloading does not reach compressive strains, the reloading curve is assumed to coincide with the unloading curve, although in reality it lies higher, exhibiting a hysteresis loop [Fig. 2(*d*)]. The reloading diagram obtained according to these rules is exemplified in Fig. 2(*c*).

Algorithm for Combined Strain Softening, Creep and Shrinkage

Since the incremental stress-strain relation (Eq. 22) is of an elastic form, the incremental problem represents an elasticity problem, which may be solved by finite elements. To improve accuracy, iterations of each time step are desirable. The computation may proceed in each time step as follows.

1. Assume suitable values for $\Delta\boldsymbol{\xi}$ for every finite element and every integration point. One may use the same values as obtained in the previous step; however, if loading reverses to unloading, then it is better to assume zero values.

2. After checking the loading-unloading-reloading criterion, compute $\lambda_{\mu_{r+1/2}}$, β_{11}, β_{22}, ... D_{11}, ... E^M, $\Delta\epsilon''_{11}$, ..., and $\Delta\xi''_{11}$, ... for every finite element and every integration point, using the stress values for the beginning of the time step, t_r. For loading, use Eqs. 8, 13, 19 and 20; for unloading, use Eqs. 8, 19, 20 and 24; and for reloading, use Eqs. 8, 19, 20 and 25.

3. Solve the elastic problem and obtain the increments of $\boldsymbol{\sigma}$ and $\boldsymbol{\epsilon}$ for every finite element and every integration point (Eqs. 22 and 23). Then find $\Delta\boldsymbol{\xi}$ from $\Delta\boldsymbol{\sigma}$, $\Delta\boldsymbol{\xi}''$ and D_{11} (Eq. 15).

4. Check if the differences of $\Delta\boldsymbol{\xi}$ values from its values in the previous iterations satisfy a given tolerance and, if they do not, iterate steps 1–4.

5. After terminating the iterations, compute the values of $\boldsymbol{\sigma}_\mu$ for the end of the step (Eq. 2). Discard the values of $\boldsymbol{\sigma}_r$ and $\boldsymbol{\sigma}_{\mu_r}$, etc., for the beginning of the step and proceed to the next step. Also, update the maximum strain values achieved so far (for later use in the unloading criterion).

Numerical studies confirmed that this algorithm is highly efficient and accurate, even for very large time steps. This is particularly so if the strain-softening curve is smooth. For a strain-softening diagram with sudden changes of slope, and especially for the case of a sudden stress drop, the convergence of the algorithm is poor and good accuracy then requires small time steps. However, the algorithm still converges. The purpose of the exponential formulas (Eqs. 11, 13, 19–21) is not to improve convergence at diminishing time steps, but to achieve very good accuracy at long time steps. For very short time steps, these formulas are equivalent to central difference formulas, and the convergence characteristics are then the same.

As far as strain softening is concerned, the use of the secant modulus C and initial strain $\Delta\xi''_{11}$ appears to be essential for convergence. Tangent incremental formulas (in which $\Delta\xi''_{11} = 0$) can be set up for strain softening; however, the solution then does not converge.

Numerical Studies and Comparison with Test Data

The uniaxial tensile strain-softening diagram [Figs. 2(*a*) and 2(*b*)] has been described earlier as $\sigma_{11} = E_s\xi_{11} \exp(-c\xi^s_{11})$ or as $\sigma_{11} = B_s\xi^q_{11} \exp(-c\xi^s_{11})$. For these expressions, the secant modulus is

$$C(\xi_{11}) = E_s e^{-c\xi^s_{11}} \quad (q = 1) \qquad (26a)$$

$$(11 \rightarrow 22 \rightarrow 33)$$

$$C(\xi_{11}) = B_s \xi^{q-1}_{11} e^{-c\xi^s_{11}} \quad (0 < q < 1) \qquad (26b)$$

in which c, s, q, E_s and B_s are empirical constants. The first equation, for which the initial tangent is inclined, includes a part of the elastic response together with the strain-softening diagram [the other part of the elastic response being given by the Maxwell chain model, Fig. 1(*f*)]. The

second equation, for which the initial tangent is vertical, includes no elastic response since the initial slope is infinite [Fig. 1(*g*)], and in this case the elastic response is totally represented by the Maxwell chain model. The existing test data are not sufficient to decide which of these two formulas should be used, and so the computer program has been written for both. From the viewpoint of convergence and accuracy, Eqs. 26*a* and 26*b* appear to work equally well if the exponential algorithm is used.

The empirical parameters in these formulas may be determined from the value of the peak stress f_t' (the tensile strength) and the corresponding value $\xi_{11} = \xi_p$ [Fig. 1(*f*)]. Setting the derivative of the curve $\sigma_{11}(\xi_{11})$ to zero, we find

$$c = \frac{1}{s}\xi_p^{-s}, \quad E_s = \frac{f_t'}{\xi_p} e^{c\xi_p^s} \qquad (27a)$$

$$c = \frac{q}{s}\xi_p^{-s}, \quad B_s = f_t' \xi_p^{-q} e^{c\xi_p^s} \qquad (27b)$$

Alternatively, parameters e and s for known (or chosen) E_s (or B and q) may also be determined by linear regression, plotting (for Eq. 26*a*) $\log [\log (E_s\xi_{11}/\sigma_{11})]$ versus $\log \xi_{11}$, or (for Eq. 26*b*) $\log [\log (E_s\xi_{11}^q/\sigma_{11})]$ versus $\log \xi_{11}$.

In the case that ξ_{11} includes a part of the elastic strain (Eq. 26*a*) equal to σ_{11}/E_s, one must subtract this value from the elastic deformation to be represented by the Maxwell chain model. Thus, the Maxwell chain parameters are calculated from the modified compliance function:

$$J^M(t,t') = J(t,t') - \frac{1}{E_s} \qquad (28)$$

as shown in Fig. 3(*b*). The algorithm for determining the Maxwell chain parameters from $J^M(t,t')$ is the same as that used for the actual compliance function $J(t,t')$ and published in Refs. 4 and 7.

It is also possible to use a bilinear stress-strain diagram with a discontinuous slope, but convergence at slope change is then poorer.

In typical practical creep problems, the time integration has to be carried out to very long times, e.g., 50 yr. The time step, therefore, is gradually increased in a geometric progression (2). Despite strain softening,

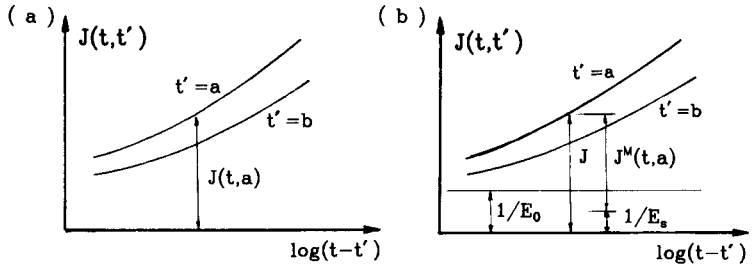

FIG. 3.—Compliance Functions and Its Modification with Reduced Instantaneous Deformation

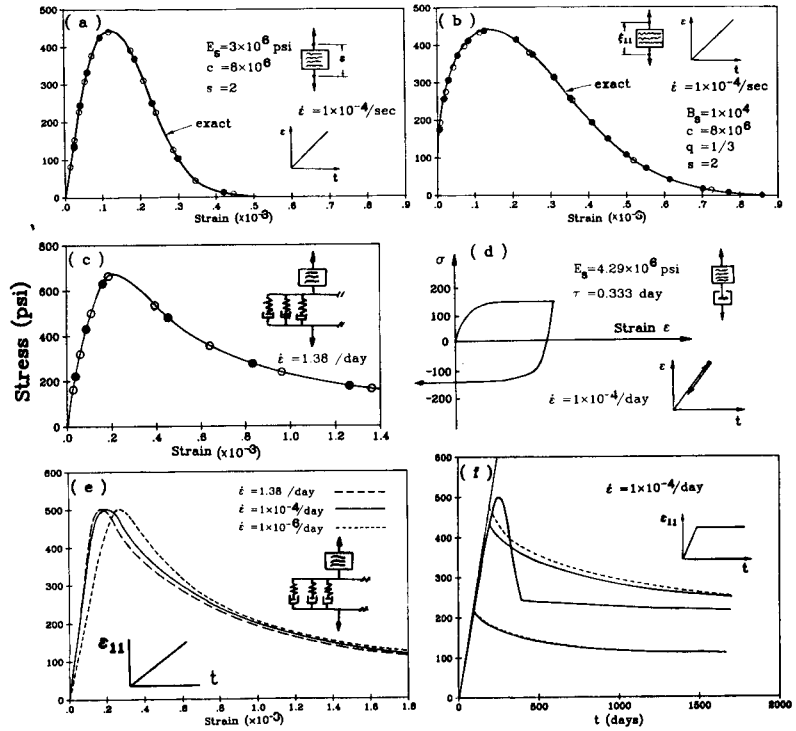

FIG. 4.—(*a*), (*b*) and (*c*): Numerical Results for Exponential Algorithm; (*d*) Response for Very Viscous Material; (*e*) Strain-Rate Effect; (*f*) Calculated Stress Relaxation Due to Constant Strain

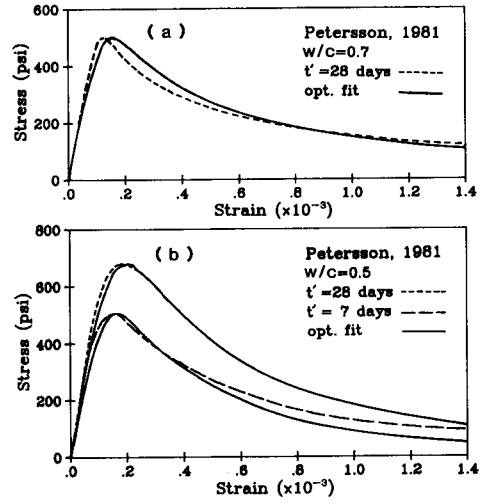

FIG. 5.—Optimal Fits of Test Data Using

the same time-stepping procedure as that explained in Refs. 2–6 has been used in computations, made possible by the exponential algorithm for strain softening. Generally, 5 time steps per decade in the logarithmic time scale have been used; the first time step was about 0.01 day.

Application of the present model in finite element analysis is described in a subsequent work (7). Here we describe various checks and numerical studies of the response obtained from the present constitutive equation for prescribed stress or strain histories.

First, the integration of the strain-softening curve $\sigma_{11}(\xi_{11})$ has been checked, setting E^M and τ_μ for the Maxwell chain at very large numbers (10^{30}). The strain ξ_{11} is increased at a constant rate, $\dot{\xi}_{11} = 10^{-4}$/sec, and various time steps, Δt, are used. The computed points are graphically indistinguishable from the specified curve $\sigma_{11}(\xi_{11})$, even though the steps are as large as those indicated by the points in the figure. Second, the behavior of the solution has been checked for finite τ_μ and E^M, i.e., with creep and aging (at constant $\dot{\xi}_{11}$), and the response has been found again to be stable and accurate, even for large steps [Figs. 4(*a*), 4(*b*) and 4(*c*)].

Next, the effect of creep, as represented by the Maxwell chain, is explored. Different strain rates, $\dot{\xi} = 1.38$, 10^{-4} and 10^{-6}/day, are now used, and the response is seen to be strain-rate dependent, although the peak stress remains constant. (In order to obtain a strain-rate effect on the peak stress, the value of f_t' would have to be adjusted according to the strain rate.) The computations are done by controlling the strain increments and solving for the stress increments. For a very viscous material, with $\tau_\mu = 0.333$ day, the creep response prevails and strain softening need not develop [Fig. 4(*d*)]. The unloading response shows then a significant hysteresis, due mostly to creep from the Maxwell chain.

The constitutive model must also be capable of representing stress relaxation due to creep. The response then differs, depending on whether strain softening has or has not been reached [Fig. 4(*f*)]. In these calculations, the strain is first rapidly increased and is then held constant, and the stress increment is solved in each time step.

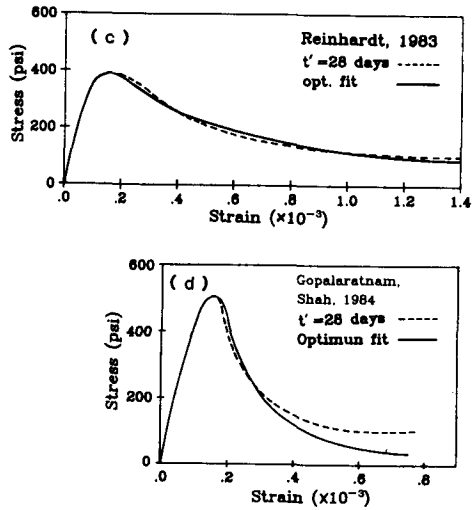

σ_{11}-ξ_{11} **Curves with Vertical Initial Slope**

TABLE 1.—Material

Data set (1)	Age of loading, t', in days (2)	Softening Parameters B_s (3)	C (4)	q (5)	S (6)	ψ (7)	f_t', in pounds per square inch (8)	Dynamic modulus (10^6 psi) (9)
Petersson 1981	7	24,515	220	0.333	0.6	0.465	507	5.8
w/c = 0.5 (*a*)	28	29,815	184.5	0.333	0.6	0.465	680	
Petersson 1981 w/c = 0.7 (*b*)	28	27,057.3	95.62	0.333	0.5	0.42	507	5.22
Reinhardt 1983 (*c*)	28	21,378.7	81.55	0.333	0.48	0.55	390	
Gopalaratnam, Shah 1984 (*d*)	28	21,780.0	1,286	0.333	0.75	0.40	505	

The aging effect on the strain-softening diagram is checked in Fig. 5(*b*). The strength, f_t', increases with age due to the hydration of cement. In the present model, however, we get an age effect on the peak stress even if f_t' is constant. This is due to the increase of the elastic moduli E_μ of the Maxwell chain units with age t. Fig. 5(*b*) shows the response curves at different ages of concrete. These curves are reasonable.

The effect of the strain rate obtained from the model [Fig. 5(*e*)] can be checked against various test data. The fact that about the same peak

TABLE 2.—Moduli (10^6 psi) and Relaxation Times (Days) for Maxwell Chain Units

Data set, from Table 1 (1)	t' (2)	t' (3)	τ_μ 0.33 (4)	3.33 (5)	33.3 (6)	333 (7)	3,333 (8)	3.3×10^4 (9)	1×10^{30} (10)
(*a*)	7 or 28	8	1.01	0.871	0.849	1.01	1.24	1.48	−2.29
		25	1.11	0.958	0.871	0.954	1.16	1.37	−1.43
		80	1.16	1.04	0.927	0.931	1.08	1.25	−0.951
		253	1.14	1.08	0.997	0.945	1.01	1.12	0.210
		800	1.07	1.09	1.05	0.986	0.983	1.01	0.935
		2,529	0.976	1.05	1.08	0.104	0.985	0.950	0.155
(*b*)	28	8	0.836	0.730	0.735	0.933	1.24	1.55	−2.48
		25	0.938	0.814	0.756	0.877	1.14	1.42	−1.600
		80	0.975	0.886	0.806	0.848	1.05	1.27	−0.704
		253	0.941	0.918	0.864	0.853	0.969	1.12	0.164
		800	0.859	0.902	0.903	0.879	0.923	0.997	0.956
		2,529	0.758	0.852	0.907	0.906	0.908	0.923	0.163
(*c*)	28	0.629 for any t' and τ_μ							
(*d*)	28	0.664 for any t' and τ_μ							

Note: Measured from stress-strain diagram, no aging involved; 1 ksi = 6.89 MPa; 1 lb/ft^3 = 16.01 kg/m^3.

Parameters for Fig. 5

E_{28} (from MATPAR, 10^6 psi) (10)	Strain rate (day^{-1}) (11)	Density of concrete, ρ (lb/ft^3) (12)	f'_c28, in kips per square inch (13)	Mix, $w:c:s:q$ (14)	Coefficients of Double Power Law				
					E_0 (15)	m (16)	n (17)	α (18)	ϕ_1 (19)
5.03	0.72	142.8	7.687	0.5:1:2:2.71	1.033E7	0.297	0.179	0.05	4.083
4.38	0.72	139.56	4.35	0.7:1:2.55:3.38	8.929E6	0.333	0.175	0.036	4.575
4.4	1.382								
4.64	0.0864			Mortar					

stresses are obtained for tensile loadings at various strain rates is confirmed by the tests of Suaris and Shah (32) and Takeda (33). However, it may be that the present model, in which the strain-rate effect is totally due to visco-elastic creep (as in the work of Bažant and Oh, Ref. 14), does not work for very high strain rates for which a solid friction mechanism may prevail (27).

The present model can be compared with the existing experimental data for the complete tensile stress-strain curve of concrete in direct tension (21,26,28), which were obtained with an accurate electronic control and monitoring system. The fits of these data are shown in Figs. 5 and 6, and the corresponding values of the material parameters are indicated in the figures and in Tables 1–4.

TABLE 3.—Material Parameters for Fig. 6

Data set (1)	MODULI (10^6 PSI) AND RELAXATION TIMES (DAY) FOR MAXWELL CHAIN UNITS							
	μ / τ_μ / t' (2)	1	2	3	4	5	6	7
		0.33 (3)	3.33 (4)	33.3 (5)	333 (6)	3,333 (7)	3.3×10^4 (8)	1×10^{30} (9)
(a)	8	1.03	0.889	0.863	1.02	1.26	1.49	−2.32
	25	1.15	0.982	0.888	0.970	1.17	1.39	−1.47
	80	1.20	1.07	0.948	0.949	1.09	1.26	−0.618
	253	1.19	1.12	1.02	0.965	1.03	1.14	0.193
	800	1.12	1.13	1.09	1.01	1.00	1.03	0.929
	2,529	1.03	1.10	1.12	1.07	1.01	0.996	1.55
(b)	8	0.848	0.738	0.742	0.940	1.25	1.56	−2.51
	25	0.955	0.826	0.764	0.885	1.15	1.43	−1.62
	80	0.996	0.901	0.817	0.857	1.06	1.28	−0.722
	252	0.965	0.937	0.879	0.863	0.980	1.13	0.152
	800	0.884	0.924	0.921	0.892	0.934	1.01	0.951
	2,529	0.782	0.874	0.928	0.923	0.921	0.933	0.163
(c)	0.630 for any t' and τ_μ							

TABLE 4.—Material Parameters for Fig. 6

Data set (1)	Age at loading, t', in days (2)	Softening Parameters			
		E_s (3)	c (4)	s (5)	ψ (6)
(a)	7	2.87×10^8	65.23	0.30	0.50
	28	2.71×10^8	58.71	0.30	0.50
(b)	28	4.35×10^8	44.79	0.25	0.55
(c)	28	2.37×10^9	33.99	0.18	0.55

To fit the measured strain-softening curves, first the values of the tensile and compressive strengths and of the composition of concrete are used to predict, with the help of the BP model (15,16), the parameters of the creep law (the double power law), and then program MATPAR (4) is used to determine the elastic moduli and relaxation times for the Maxwell chain units. Next, the elastic and creep properties being fixed, various values of parameters s, q and ξ_p are tried, along with the corresponding value of B_s (Eq. 27*b*), until the best fit of the measured tensile stress-strain diagram is obtained.

If the curve $\sigma_{11}(\xi_{11})$ with a finite initial slope (Eq. 26*a*) is used, determination of the compliance function from the given tensile and compressive strengths and concrete composition must be followed by a choice of modulus E_s for Eq. 26*a*. To obtain parameters of the Maxwell chain, the modified compliance function $J^M(t,t')$ and program MATPAR (4) are used. Then, various values of s or ξ_p, with the corresponding value of c determined from Eq. 27*a*, are tried until the best fit of the tensile stress-strain curve is found.

Fig. 7 shows the effect of exponent s on the shape of the tensile stress-strain curve (Eq. 27*b*). This knowledge is useful for data fitting. For large exponents, such as $s \geq 2$, the tensile strain curve exhibits a nearly vertical stress drop. The solution converges even then, although the accuracy is poorer (but still acceptable).

By analysis of the existing test d (10,26,28), approximate empirical formulas to predict the values of t aterial parameters for the strain-softening curve have been found. the curve $\sigma_{11}(\xi_{11})$ with initial vertical tangent, these formulas are

$$s = 0.55, \quad \xi_p \simeq \frac{f'_t}{2E_{28}}, \quad c \simeq 0.89\left(\frac{E_{28}}{f'_t}\right. \quad E_s \simeq 2.3f'_t\left(\frac{E_{28}}{f'_t}\right)^q, \quad q \simeq \frac{1}{3} \qquad (29)$$

in which E_{28} is the conventional st lastic modulus at age 28 days. For the curve $\sigma_{11}(\xi_{11})$ with an initia ent of finite slope (Eq. 26*a*)

$$s = \frac{1}{4}, \quad \xi_p = \frac{0.55f'_t}{E_{28}}, \quad c \simeq 4.645\left(\frac{E_{28}}{f'_t}\right)^{0.} \quad \simeq 99.27E_{28} \ldots\ldots\ldots\ldots \qquad (30)$$

The tensile stress-strain curve predicted u these values is plotted in Figs. 8 and 9. Alternatively, a previously loped formula for predicting fracture energy G_f (14) may be u d. Then the foregoing expressions for s should be deleted and s n found from the con-

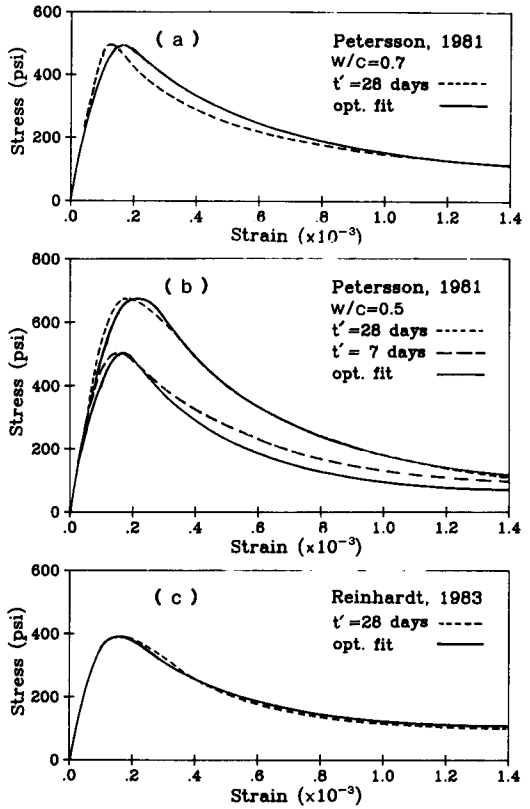

FIG. 6.—Optimal Fits of Test Data Using σ_{11}-ξ_{11} Curves with Finite Initial Slope

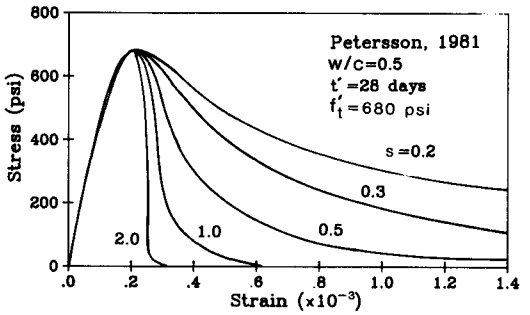

FIG. 7.—Effect of Exponent s on Tensile Stress-Strain Curve (Eq. 26*a*)

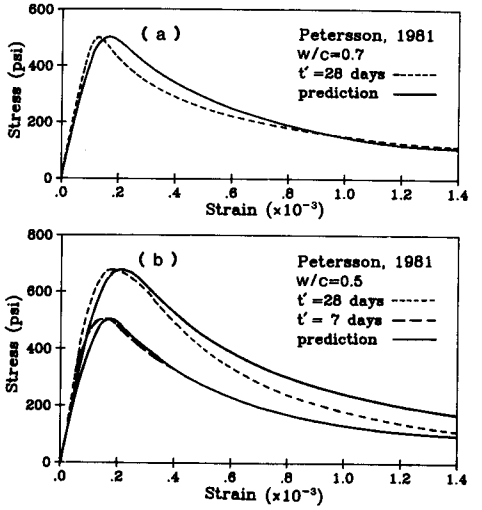

FIG. 8.—Predictions Compared with Test Data

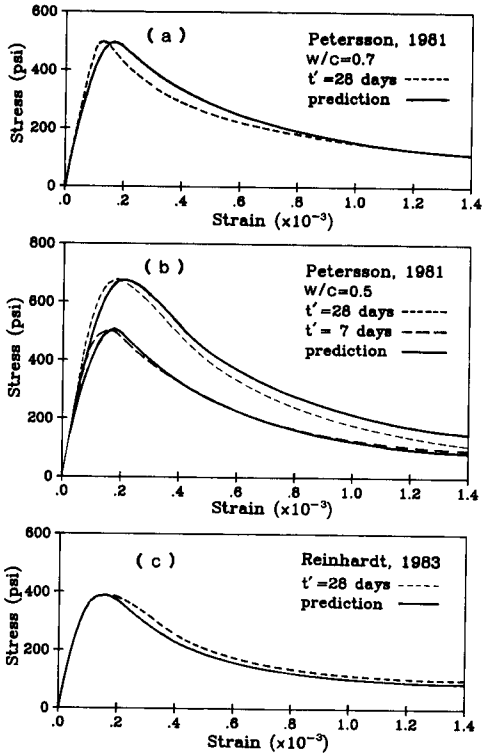

FIG. 9.—Predictions Compared with Test Data for σ_{11}-ξ_{11} Curves with Finite Initial Slope

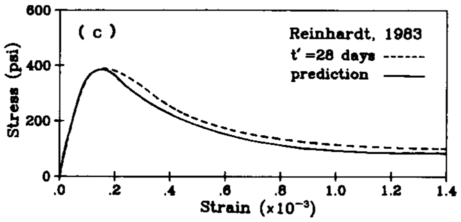

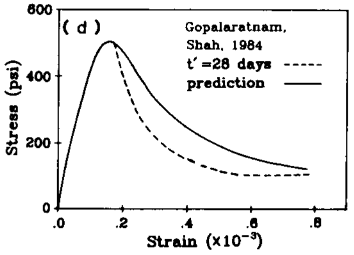

for σ_{11}-ξ_{11} Curves with Vertical Initial Slope

dition that the area under the $\sigma_{11}(\xi_{11})$ curve equals G_f/w_c, in which $w_c \simeq 3d_a$ and d_a = maximum aggregate size (14).

Conclusions

1. The condition that, for any loading path, strain softening must lead at large strains to a reduction of stress to exactly zero is easily satisfied by using an algebraic relation between the stress and the strain associated with microcracking.

2. To assure that, for compressive or small tensile strains, the constitutive model reduces to a simple model for creep with elastic deformation, and that, at sufficiently large tensile strain, the stress is reduced to exactly zero, regardless of creep or shrinkage, strain softening may be represented as an additional strain caused by the same stress as creep. In a rheologic model, this is visualized by a strain-softening element coupled in series with the element that describes creep with elastic deformation and shrinkage.

3. If microcracking is restricted to occur only in three orthogonal planes, strain softening may be described independently for each of three orthogonal directions, and the loading and unloading criteria may also be considered independent for each of these three directions.

4. Realistic unloading curves are obtained by assuming that the tangent of the unloading curve has the same slope as the secant of the loading curve for the same value of the strain. In the differentiated form of the stress-strain relation, this simply corresponds to dropping the inelastic stress increment when unloading takes place. The exponential algorithm has a self-correcting property in that the stress is reduced at very large strain exactly to zero, even if a numerical error is previously accumulated.

5. An efficient step-by-step integration is made possible by the exponential algorithm, which uses within each time step an exact solution of the differentiated stress-strain relation considered as a quasi-viscoelastic first-order linear differential equation for stress with constant coefficients. The values of the coefficients are assumed to change discontinuously between the time steps.

6. The exponential algorithm, in a manner similar to other algorithms, can be formulated in terms of a pseudo-elastic incremental stress-strain relation for the strain-softening part of strain and, in this form, can be combined with the previously developed exponential algorithm for a linear, aging, rate-type creep law. This algorithm is not only accurate for very large time steps, but also assures that stress approaches exactly zero as the tensile strain increases to large values for any loading path, regardless of creep and shrinkage. For very small time steps, the exponential algorithm is equivalent to secant central difference formulas, which, however, do not work for large time steps. Solution is also possible with tangential incremental pseudo-elastic relations for strain softening; however, the loading steps must be extremely short.

7. The combined strain-softening creep model seems to give reasonable strain-rate and aging effects for the complete tensile stress-strain curves, and also to yield reasonable creep curves, stress relaxation and creep recovery. However, precise test data are lacking to verify this.

8. The tensile strain-softening data available in the literature can be well-represented with the present model.

Acknowledgment

Financial support under U.S. National Science Foundation Grant No. CEE800-3148 to Northwestern University is gratefully acknowledged. Thanks are also due to Mary Hill for her outstanding secretarial assistance.

Appendix I.—Strain-Softening Model for Cracking in All Directions

It is possible to generalize the present model so that cracking of any orientation will be permitted. The condition that, for sufficiently large normal strains of any direction, the associated normal stress must reduce exactly to zero can be easiest satisfied if the stress-strain relation which governs strain softening is path-independent, i.e., if a deformation potential, $\Phi(\xi)$, exists and the stress is expressed as

$$\sigma_{ij} = \frac{\partial \Phi(\xi)}{\partial \xi_{ij}} \quad (32)$$

The uniaxial strain-softening diagrams are then of the same type as considered before if the potential function is expressed as

$$\Phi(\xi) = -k_1 e^{-k_0(\xi_1+\xi_2+\xi_3)^s} - k_2(e^{-k\xi_1^s} + e^{-k\xi_2^s} + e^{-k\xi_3^s}) \quad (s \le 2) \quad (33)$$

in which k, k_0, k_1, k_2 and s are empirical constants; and ξ_1, ξ_2 and ξ_3 are the principal values of tensor ξ_{ij}. Eq. 33 satisfies the condition of

isotropy. In a manner equivalent to Eq. 32, the constitutive relation can be described by secant moduli C_{ijkm}:

$$\sigma_{ij} = C_{ijkm}(\xi)\xi_{km}, \quad C_{ijkm}(\xi) = \left(\frac{\partial\Phi}{\partial\xi_{pq}}\xi_{pq}\right)^{-1}\frac{\partial\Phi}{\partial\xi_{ij}}\frac{\partial\Phi}{\partial\xi_{km}} \quad \ldots\ldots\ldots\ldots\ldots\ldots (34)$$

If unloading is assumed to be governed by tangential moduli that equal the secant moduli for loading, then $d\sigma_{ij} = C_{ijkm}(\xi)d\xi_{km}$.

The condition of path independence of the foregoing relations means, from the physical viewpoint, that the opening, density and orientation of microcracks uniquely characterize the overall stress in the material. This is no doubt a simplification. From the numerical viewpoint, Eq. 32 has the disadvantage that an efficient time-step algorithm cannot be easily formulated. Furthermore, the transition from loading to unloading has an undesirable property—the dependence of incremental stiffness of the load increment direction if the stress space is not continuous in regard to the orientation of this increment. The unloading condition can no longer be treated separately for various directions.

Appendix II.—References

1. Anderson, C. A., "Numerical Creep Analysis of Structures," *Creep and Shrinkage in Concrete Structures*, Z. P. Bažant and F. H. Wittman, eds., John Wiley and Sons, Ltd., 1982, p. 259.
2. Bažant, Z. P., "Mathematical Models for Creep and Shrinkage of Concrete," *Creep and Shrinkage in Concrete Structures*, Chapter 7, Z. P. Bažant and F. H. Wittmann, eds., John Wiley and Sons, 1982, pp. 163.
3. Bažant, Z. P., "Numerically Stable Algorithm with Increasing Time Steps for Integral-Type Aging Creep," *Proceedings of the First International Conference on Structural Mechanics in Reactor Technology* (SMiRT1), held in West Berlin, Germany, Sept., 1971, by T. A. Jaeger, ed., Commission of European Communities, Brussels, Belgium, Vol. 4, Part H, pp. 119–126.
4. Bažant, Z. P., "Input of Creep and Shrinkage Characteristics for a Structural Analysis Program," *Materials and Structures*, (RILEM, Paris, France), *15*, No. 88 283, 1982.
5. Bažant, Z. P., "Theory of Creep and Shrinkage in Concrete Structures: A Précis of Recent Developments," *Mechanics Today*, S. Nemat-Nasser, ed., Vol. 2, John Wiley and Sons, Inc., New York, N.Y., 1975, pp. 1–93.
6. Bažant, Z. P., "Mechanics of Fracture and Progressive Cracking in Concrete Structures," *Fracture Mechanics Applied to Concrete Structures*, Chapter I, G. C. Sih and V. DiTomasso, eds., Vol. 2, Martinus Nijhoff Publishers, The Hague, The Netherlands, 1984.
7. Bažant, Z. P., and Chern, J. C., "Concrete Creep at Variable Humidity: Constitutive Law and Mechanism," *Report No. 84-4/679t*, Center for Concrete and Geomaterials, Northwestern University, Evanston, Ill., 1984.
8. Bažant, Z. P., and Chern, J. C., "Rate-Type Concrete Creep Law with Reduced Time," *Journal of Engineering Mechanics*, ASCE, Vol. 110, No. 3, March, 1984.
9. Bažant, Z. P., and Gambarova, P. G., "Crack Shear in Concrete: Crack Band Microplane Model," *Journal of Engineering Mechanics*, ASCE, 1984 (in press).
10. Bažant, Z. P., and Oh, B. H., "Deformation of Progressively Cracking Reinforced Concrete Beam," *ACI Journal*, Vol. 81, No. 3, 1984, pp. 268–278.
11. Bažant, Z. P., and Oh, B. H., "Microplane Model for Fracture Analysis of Concrete Structures," *Proceedings of the Symposium on the Interaction of Non-Nuclear Munitions with Structures*, held at the U.S. Air Force Academy, May, 1983, pp. 49–55.

12. Bažant, Z. P., and Oh, B. H., "Crack Band Theory for Fracture of Concrete," *Matériaux et Constructions* (RILEM, Paris), Vol. 16, No. 93, 1983, pp. 155–177.
13. Bažant, Z. P., "Crack Band Model for Fracture of Geomaterials," *Proceedings of the 4th International Conference on Numerical Methods in Geomechanics*, held in Edmonton, Alberta, Canada, 1982, Z. Eisenstein, ed., Vol. 3, pp. 1137–1152.
14. Bažant, Z. P., and Oh, B. H., "Strain Rate Effect in Rapid Triaxial Loading of Concrete," *Journal of the Engineering Mechanics Division*, ASCE, Vol. 108, Oct., 1982, pp. 764–782.
15. Bažant, Z. P., and Panula, L., "Practical Prediction of Time-Dependent Deformation of Concrete," *Materials and Structures*, Parts I and II: *11*, No. 65, 307, 1978; Parts III and IV: *11*, No. 66 415, 1978; Parts V and VI: *12*, No. 69, 169, 1979.
16. Bažant, Z. P., and Panula, L., "Creep and Shrinkage Characterization for Analyzing Prestressed Concrete Structures," *Journal of the Prestressed Institute*, Vol. 25, May–June, 86, 1980, pp. 86–122.
17. Bažant, Z. P., and Raftshol, W. J., "Effect of Cracking in Drying and Shrinkage Specimens," *Cement and Concrete Research*, Vol. 12, 1982, pp. 209–226.
18. Bažant, Z. P., and Wu, S. T., "Creep and Shrinkage Law for Concrete at Variable Humidity," *Journal of the Engineering Mechanics Division*, ASCE, Vol. 100, 1974, pp. 1183–1209.
19. Bažant, Z. P., and Wu, S. T., "Rate-Type Creep Law of Aging Concrete Based on Maxwell Chain," *Matériaux et Constructions* (RILEM, Paris), Vol. 7, 1974, pp. 45–60.
20. Evans, R. H., and Marathe, M. S., "Microcracking and Stress-Strain Curves for Concrete in Tension," *Matériaux et Constructions* (RILEM, Paris), No. 1, Jan.–Feb., 1968, pp. 61–64.
21. Gopalaratnam, V. S., and Shah, S. P., "Softening Response of Concrete in Direct Tension," *ACI Journal*, 1984 (in press).
22. Heilmann, H. C., Hilsdorf, H., and Finsterwalder, I., "Strength and Deformation of Concrete Under Tensile Stress," *Deutscher Ausschuss für Stahlbeton*, Heft 203, W. Ernst and Son, Berlin, Germany, 1969 (in German).
23. Hughes, B. P., and Chapmann, B. P., "The Complete Stress-Strain Curve for Concrete in Direct Tension," *RILEM Bulletin No. 30*, 1966, pp. 95–97.
24. Iding, R., and Bresler, B., "Prediction of Shrinkage Stresses and Deformations in Concrete," *Fundamental Research on Creep and Shrinkage of Concrete*, F. H. Wittmann, ed., Martinus Nijhoff, 1982, pp. 397.
25. Kabir, A. F., and Scordelis, A. C., "Analysis of RC Shells for Time Dependent Effects," *IASS Bulletin XXI*, No. 69, 1979.
26. Petersson, P. E., "Crack Growth and Development of Fracture Zones in Plain Concrete and Similar Materials," *Report TVBM 1006*, Lund Institute of Technology, Lund, Sweden, Dec., 1981.
27. Pozzo, E., "Rheological Model of Concrete in the Dynamic Field," *Meccanica*, Vol. 5, June, 1970, pp. 143–158.
28. Reinhardt, H. W., Cornelissen, H. A. W., "Post-Peak Cyclic Behavior of Concrete in Uniaxial Tensile and Alternating Tensile and Compressive Loading," *Cement and Concrete Research*, Vol. 14, pp. 263–270, 1984 [also see *IUTAM Prager Symposium on Mechanics of Geomaterials*, held in Evanston, Ill., 1983 (preprints edited by Z. P. Bažant), pp. 638–642].
29. Roelfstra, P. E., "Computerized Structural Analysis Applied to Large-Span Bridge," *Fundamental Research on Creep and Shrinkage of Concrete*, F. H. Wittmann, ed., Martinus Nijhoff, 1982, pp. 407–427.
30. Rüsch, H., Hilsdorf, H., "Deformation Characteristics of Concrete under Axial Tension," *Bericht Nr. 44* des MPA Bauwesen der T. H. München, 1963 (in German).
31. "State-of-the-Art Report on Finite Element Analysis of Concretes," by the ASCE Task Committee on Finite Element Analysis of Concrete Structures, A. H. Wilson, Chmn., New York, N.Y., 1982.
32. Suaris, W., and Shah, S. P., "Properties of Concrete Subjected to Impact,"

Journal of Structural Engineering, ASCE, Vol. 109, No. 7, July, 1983, pp. 1727–1741.
33. Takeda, J., and Tachikawa, H., "Deformation and Fracture of Concrete Subjected to Dynamic Load," *Proceedings of International Conference on Mechanical Behavior of Materials*, Vol. IV, Concrete and Cement Paste, Glass and Ceramics, Kyoto, Japan, Aug., 1971, pp. 267–277.
34. Wittmann, F. H., and Roelfstra, P. E., "Total Deformation of Loaded Drying Concrete," *Cement and Concrete Research*, Vol. 10, 1980, pp. 601–610.